CHEMISTRY OF MATERIALS

pubs.acs.org/cm

Article

Three-Dimensional Printable, Extremely Soft, Stretchable, and Reversible Elastomers from Molecular Architecture-Directed Assembly

Shifeng Nian,[#] Jinchang Zhu,[#] Haozhe Zhang, Zihao Gong, Guillaume Freychet, Mikhail Zhernenkov, Baoxing Xu, and Li-Heng Cai*

Cite This: *Chem. Mater.* 2021, 33, 2436−2445

Read Online

ACCESS | Metrics & More | Article Recommendations | Supporting Information

ABSTRACT: 3D printing elastomers enables the fabrication of many technologically important structures and devices such as tissue scaffolds, sensors, actuators, and soft robots. However, conventional 3D printable elastomers are intrinsically stiff; moreover, the process of printing often requires external mechanical support and/or post-treatment. Here, we exploit the self-assembly of a responsive linear-bottlebrush-linear triblock copolymer to create stimuli-reversible, extremely soft, and stretchable elastomers and demonstrate their applicability as inks for *in situ* direct-write printing 3D structures without the aid of external mechanical support or post-treatment. By developing a procedure for controlled synthesis of such architecturally designed block copolymers, we create elastomers with extensibility up to 600% and Young's moduli down to ~10^2 Pa, 10^6 times softer than plastics and more than 10^2 times softer than all existing 3D printable elastomers. Moreover, the elastomers are thermostable and remain to be solid up to 180 °C, yet they are 100% solvent-reprocessable. Their extreme softness, stretchability, thermostability, and solvent-reprocessability bode well for future applications.

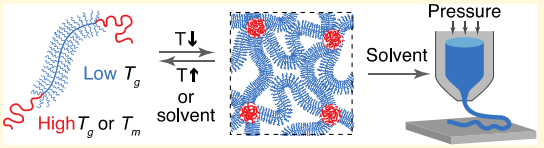

INTRODUCTION

Additive manufacturing, or 3D printing, produces customized objects by combining computer-aided design with 3D printing techniques, and it can create multi-length scale structures inaccessible by conventional molding.[1−3] Plastics, such as photocurable resins, thermoplastics, and thermosets, are the most ubiquitous feedstock for desktop and industrial 3D printers.[2,4,5] All these materials are not only stiff with Young's moduli of 10^8−10^{10} Pa but also fragile with extensibility often below 10%;[5] such high stiffness and low extensibility severely limit their application as adaptive materials that comply with the shapes of objects they contact. By contrast, elastomers are much softer and more deformable. Thus, it has been innovated in both technology[6−8] and materials development[9−12] to 3D print elastomers, based on which adaptive structures and devices such as tissue scaffolds,[13,14] sensors,[15] actuators,[16,17] and soft robots are created.[8,18] Basic materials, however, are limited to thermo-reversible liquid crystal elastomers and a few photo- or thermo-curable elastomers.[16,19−21] Although the moduli of these elastomers, 10^6−10^8 Pa, are much lower than those of plastics, they remain orders of magnitude higher than those of ultrasoft biological tissues, 10^2−10^5 Pa.[22] Further lowering the stiffness of polymer networks may significantly broaden their applications, and a notable example is soft hydrogels that are widely used as basic materials for biomedicine and stretchable electronics.[23−25] However, hydrogels contain a large amount of water that can evaporate or leach out and in doing so will deteriorate material properties. As a result, it is of great technological importance to develop 3D printable, ultrasoft, yet solvent-free elastomers.

Previously, we reported a class of ultrasoft, solvent-free elastomers by covalently cross-linking bottlebrush rather than linear polymers.[26] Compared to a linear polymer, a bottlebrush polymer has a significantly higher entanglement molecular weight.[27] This not only prevents the formation of entanglements but also enables low density of cross-links, resulting in solvent-free elastomers of extreme softness with prescribed Young's moduli from ~10^4 to ~10^6 Pa, comparable to that of "watery" biological tissues. This concept has been further exploited by other groups to create ultrasoft elastomers.[28,29] However, the covalent cross-links are permanent and prevent shear-induced solid-to-liquid transition, a property required for materials being used as inks for direct-write printing, a 3D printing technique that is widely available and capable of transforming highly viscoelastic inks to functional structures such as magnetic[18] and pneumatic[8] robots. To 3D print bottlebrush-based elastomers, very recently, an ink has been developed consisting of bottlebrush polymers, which, after being printed, are photo-cross-linked by premixed cross-linking agents.[30] However, photo-cross-linking is sensitive to the intensity of light, which inevitably will be attenuated as the size of printed objects

Received: December 5, 2020
Revised: March 10, 2021
Published: March 31, 2021

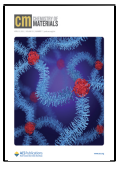

https://doi.org/10.1021/acs.chemmater.0c04659
Chem. Mater. 2021, 33, 2436−2445

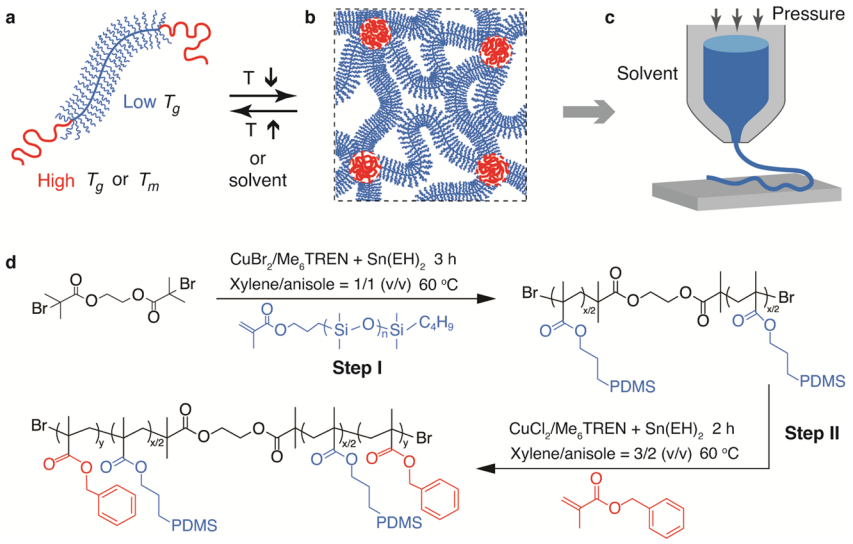

Figure 1. Design concept and synthesis of 3D printable, reversible, ultrasoft, and stretchable elastomers. (a) Schematic of a responsive linear-bottlebrush-linear triblock copolymer. (b) At low temperature, the middle bottlebrush blocks (blue) act as elastic network strands, whereas the high T_g end linear blocks aggregate to form spherical glassy domains. (c) Glassy domains dissociate at high temperature or in the presence of solvents, resulting in a solid-to-liquid transition of the network. The stimuli-triggered reversibility allows the elastomers for direct-write 3D printing. (d) Synthesis of linear-bottlebrush-linear triblock copolymers using ARGET ATRP. The side chain of the middle bottlebrush block is linear polydimethylsiloxane (PDMS), whereas the end blocks are linear poly(benzyl methacrylate) (PBnMA). A bottlebrush-based triblock polymer is denoted as $BnMA_y$-*b*-$PDMS_x^w$-*b*-$BnMA_y$, in which *y* is the number of repeating BnMA units, *x* is the number of PDMS side chains per bottlebrush, and *w* represents the MW of PDMS side chains in kg/mol. The weight fraction of the end blocks in the triblock copolymer is kept below 6% to ensure that the bottlebrush-based ABA triblock copolymers self-assemble to a sphere phase.

increases; this may result in uncontrollable cross-linking and thus mechanical properties. It has yet to be developed a 3D printable, ultrasoft elastomers without the need for post-treatment.

Recently, we developed soft, solvent-reprocessable elastomers by exploiting the self-assembly of linear-bottlebrush-linear (LBBL) triblock copolymers.[31] In an LBBL triblock copolymer, the linear blocks are a polymer of relatively high glass transition temperature T_g, whereas the middle block is a bottlebrush polymer with a linear backbone densely grafted by low T_g linear polymers (Figure 1a). At room temperature, the triblock copolymer microphase separates to a network structure, in which cross-links are spherical hard glassy domains formed by the high T_g end blocks, whereas the soft elastic network strands are the low T_g bottlebrush polymer (Figure 1b). Above the melting point of the end blocks or in the presence of solvents, the glassy domains can dissociate such that the solid network becomes liquid-like. Therefore, it is expected that such a stimuli-triggered solid-to-liquid transition allows the physically cross-linked elastomers for direct-write 3D printing (Figure 1c).

Here, we extend this design concept to create a class of stimuli-reversible, extremely soft, and stretchable elastomers and demonstrate their applicability to direct-write printing 3D structures without the aid of external mechanical support or post-treatment. By developing a procedure for controlled synthesis of such architecturally designed block copolymers, we create extremely soft elastomers with tunable Young's moduli from $\sim 10^2$ to 10^4 Pa. The lower limit, $\sim 10^2$ Pa, is $>10^6$ times softer than plastics, $>10^4$ times softer than conventional 3D printable elastomers, and $\sim 10^2$ softer than the very recently reported photo-cross-linked bottlebrush elastomers.[30] Interestingly, compared to chemically cross-linked bottlebrush elastomers,[32] the self-assembled elastomers are less stretchable because of microphase separation-induced pre-stretching of the bottlebrush network strands. Nevertheless, the extensibility of the physically cross-linked networks can be tuned in a range of 200−600%, comparable to that of existing 3D printable elastomers. Moreover, the elastomers are thermostable and remain to be solid up to 180 °C, yet they are 100% solvent-reprocessable. Their extreme softness, stretchability, thermostability, and solvent-reprocessability bode well for future applications.

RESULTS AND DISCUSSION

We use polydimethylsiloxane (PDMS) and poly(benzyl methacrylate) (PBnMA) as the two polymer species to create the linear-bottlebrush-linear ABA triblock copolymer (Figure 1d). We select PDMS and PBnMA because of two reasons. First, PDMS has an extremely low glass transition temperature $T_{g,PDMS}$ of −125 °C whereas PBnMA has a $T_{g,PBnMA}$ of 54 °C and a melting temperature $T_{m,PBnMA}$ of 200 °C.[33] Such a large difference between $T_{g,PDMS}$ and $T_{m,PBnMA}$ ensures that the self-assembled network is thermostable within a wide range of temperature. Second, reminiscent of PDMS and polystyrene,[31] PDMS and PBnMA are highly incompatible to result in a strongly segregated microphase separation. Compared to the weak segregation limit, a strongly segregated microstructure is less sensitive to annealing conditions and thus would result in more controllable macroscopic properties.[34]

We synthesize PBnMA-bottlebrush PDMS (bbPDMS)-PBnMA triblock copolymers using a two-step procedure, which involves the synthesis of first the middle bbPDMS block and then the two linear PBnMA blocks (Figure 1d). A linear PDMS polymer of a relatively large molecular weight (MW), 5000 g/mol, is used as the macromonomer, or the side chain, of the bottlebrush. The entanglement MW of the bottlebrush of such a molecular architecture is about 10^8 g/mol;[26] this high value ensures that all the samples explored in this study are unentangled. It is difficult, however, to synthesize

https://doi.org/10.1021/acs.chemmater.0c04659
Chem. Mater. 2021, 33, 2436−2445

Table 1. Molecular Parameters and Mechanical Properties of the 3D Printable, Ultrasoft, Stretchable Elastomers[a]

	middle block			triblock			mechanical properties		microstructure
sample	M_{sc} (kg/mol)	n_{BB}	PDI	n_{end}	f	PDI	γ_s	G (Pa)	d (nm)
S_{100}	5	21	1.10	17	0.06	1.33	NA	NA	NA
S_{200}	5	44	1.27	37	0.06	1.44	3.46	946	20.9 ± 4.6
S_{250}	5	50	1.15	45	0.06	1.20	2.53	4360	22.4 ± 6.6
S_{500}	5	112	1.41	109	0.06	1.52	1.66	6082	44.9 ± 8.8
S_{1000}	5	216	1.56	95	0.03	1.82	3.46	244	57.1 ± 12.7
S_{1500}	5	300	1.63	176	0.04	2.05	5.62	57	66.8 ± 22.9

[a] M_{sc}, molecular weight of side chains; n_{BB}, number of side chains per bottlebrush; n_{end}, number of chemical repeating units for the end linear PBnMA block; f, weight fraction of the end blocks; PDI, polydispersity index; G, shear modulus; γ_s, shear fracture strain of the elastomers; d, average distance between the centers of two neighboring spherical domains.

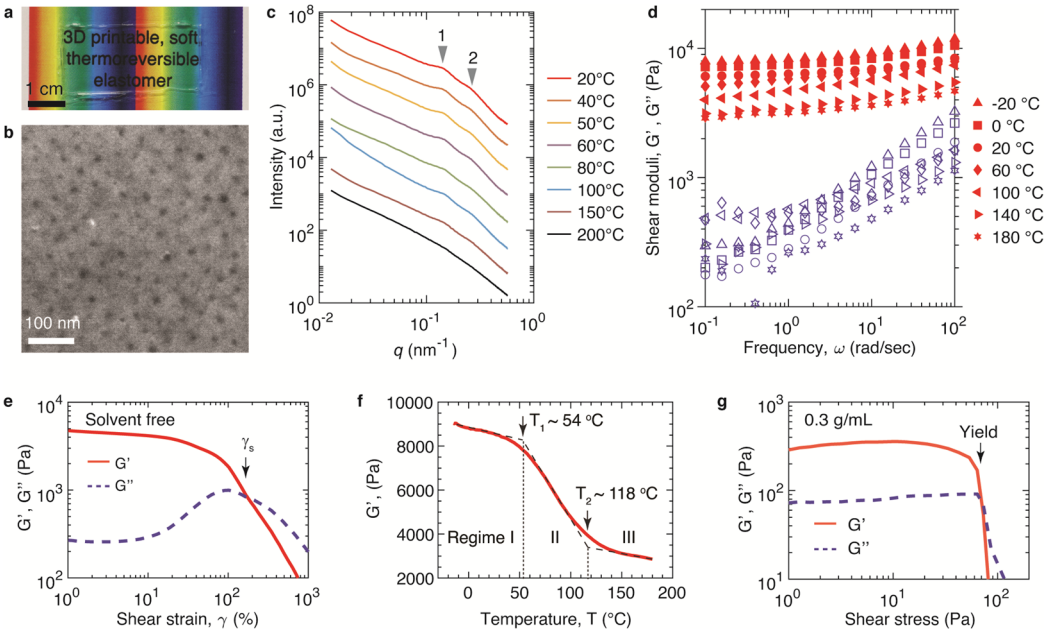

Figure 2. Self-assembled network is an optically transparent, soft, stretchable, and reversible elastomer. (a) Optical image of the elastomer self-assembled by sample S_{500}, $BnMA_{109}$-*b*-$PDMS_{112}$[5]-*b*-$BnMA_{109}$, with a molecular weight of nearly 500 kg/mol. (b) Representative image of the elastomer characterized by hollow-cone dark field TEM without staining. The dark spherical dots are domains formed by PBnMA, whereas the white region is bbPDMS. (c) *In situ* GISXAS measurements for sample S_{500} reveal the primary characteristic peak at a wavenumber of $q = 0.14$ nm^{-1} and a secondary peak at 0.29 nm^{-1} (see SI Text). Both peaks disappear at a high temperature 200 °C. (d) Frequency dependence of the storage (red symbols, G') and loss (blue symbols, G'') moduli of the soft elastomer measured at a fixed strain of 0.5% and various temperatures from −20 to 180 °C, the highest temperature accessible by our rheometer. (e) Large amplitude oscillatory shear measurements of the elastomer at 20 °C at a fixed frequency of 1 rad/s. Above a shear fracture strain, γ_s, of 1.66, G'' becomes larger than G'. (f) As the temperature increases, the network storage modulus decreases and exhibits three regimes. Regime I: $T < T_1 \sim T_{g,PBnMA} = 54$ °C, slow decrease; regime II: $T_1 < T < T_2 = 118$ °C, fast decrease; regime III: $T > T_2 \gg T_{g,PBnMA}$, slow decrease. Measurements are performed at a fixed strain of 5% and an oscillatory frequency of 1 rad/s. (g) When the elastomer is mixed with dichloromethane at a volume ratio of 1:2, the mixture is a yield stress fluid that transitions from solid-like to liquid-like at shear stresses above 70 Pa.

bottlebrush polymers of long side chains and high MW. The strong steric repulsion between the densely grafted long side chains geometrically hinders the addition of macromonomers to the propagating bottlebrush, and this steric hindrance becomes more pronounced in good solvents. In addition, the solubility of polymers decreases with the increase in molecular weight. Moreover, PDMS and PBnMA are intrinsically immiscible without cosolvents. To overcome these challenges, we extend our previous procedure for the synthesis of bottlebrush polymers,[31] but in each step, we use different cosolvents with carefully adjusted solvent quality to mitigate the steric repulsions from the densely grafted side chains while ensuring the solubility of final products (see the Experimental Section). For all polymers, we confirm chemical synthesis by nuclear magnetic resonance (NMR) spectroscopy, quantify number average MW based on the conversion rate measured by NMR, and determine polydispersity index (PDI) by gel permeation chromatography (GPC) (Figures S1 and S2 and SI Text). The parameters for all samples are listed in Table 1. For example, for a sample S_{500} with a MW about 500 kg/mol, the PDI values of the bottlebrush middle block and the triblock copolymer are 1.41 and 1.52, respectively. These results demonstrate that the synthesis procedure allows for the controlled synthesis of bottlebrush-based ABA triblock copolymers.

The self-assembled polymer at room temperature is a solid optically transparent to the full spectra of visible light, as shown by sample S_{500} in Figure 2a. Microscopically, the triblock copolymer microphase separates to form a sphere microstructure, as shown by the dark dots in a transmission electron microscopy (TEM) image (Figure 2b). The average diameter D

https://doi.org/10.1021/acs.chemmater.0c04659
Chem. Mater. 2021, 33, 2436−2445

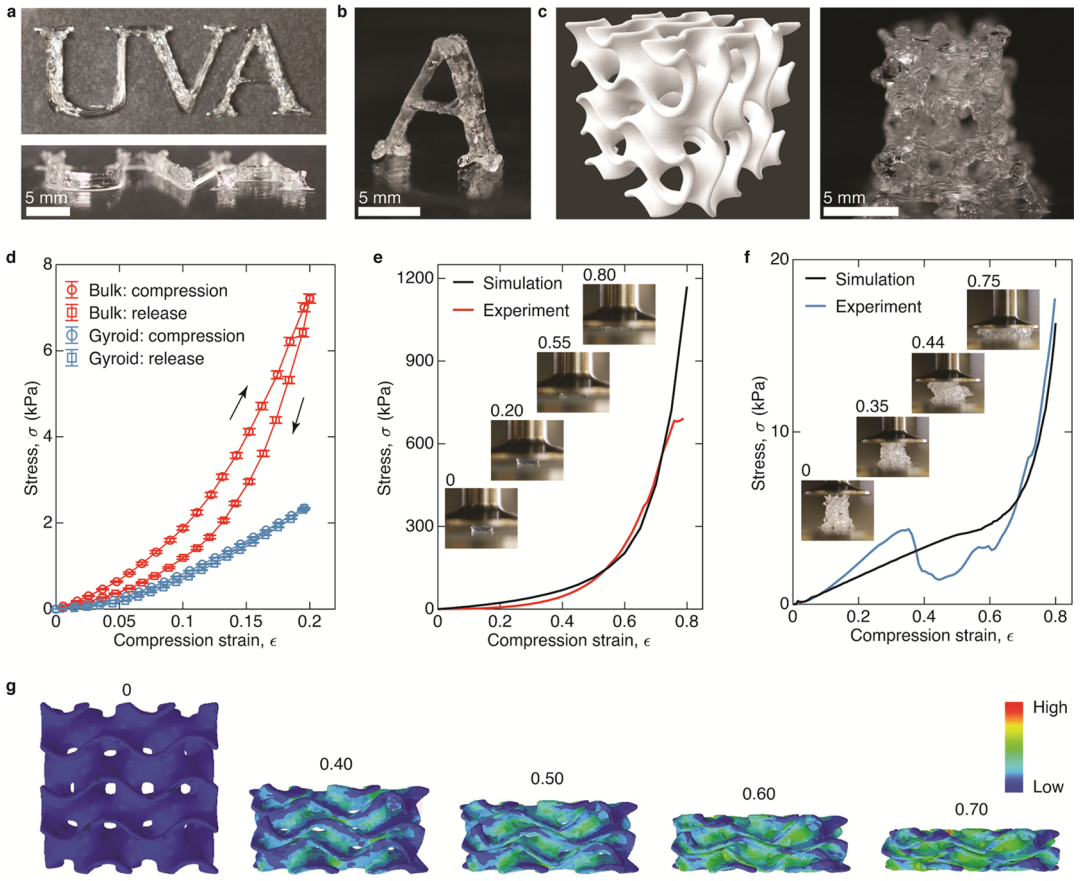

Figure 3. Direct-write printing soft elastomers to create deformable 3D structures. (a) 3D printed UVA initials with a stack thickness of 2 mm. Upper: bird's eye view; lower: side view. (b) Free-standing, 3D printed letter "A". (c) 3D rendering of a cubic gyroid (left) and the corresponding printed product with dimensions $10 \times 10 \times 10$ mm^3 (right). (d) For the bulk sample, the compression−release profile exhibits a hysteresis associated with 23% energy dissipation (dashed lines), whereas for the gyroid, there is almost no energy dissipation, as evidenced by the complete overlap between the compression and release profiles (solid lines). The apparent Young's modulus, $E = \sigma/\varepsilon$, of the gyroid is about 8 kPa, nearly a half of 20 kPa for the bulk; this is likely because the porous gyroid has a lower density about 1/2 of the bulk. The strain rate is 0.005/s. Error bar: standard deviation for $n = 5$. (e) As the compression strain increases from 0.2 to 0.55, the bulk sample exhibits strain-stiffening with the compression stress increasing from 8 to 130 kPa, and further compression with $\varepsilon > 0.55$ results in material fracture (optical images). The stress−strain profile is used to calibrate FEA simulation (dashed line). (f) Cubic gyroid exhibits a nearly linear elastic deformation up to $\varepsilon = 0.35$, at which the stress is about 5 kPa, 10 times lower than the 50 kPa for the bulk. Slightly above $\varepsilon = 0.35$, the stress exhibits a sharp decrease (solid line). (g) Decrease is associated with structural collapse of the gyroid, as indicated by comparing the snapshots from FEA simulation (dashed line in (f) and upper panel) with the optical images of the gyroid (lower panel) under various extents of compression. The use of UVA initials in 3D printing is under the permission from the UVA Office of Trademark and Licensing.

of a spherical domain is 20.4 ± 2.4 nm, and the neighboring center-to-center domain distance d is 49.2 ± 4.7 nm (Figure S3a,b). Based on the domain diameter and distance, the calculated weight fraction of the PBnMA blocks, $\sim(d/D)^3 \approx 0.06$, is consistent with that obtained from molecular parameters (Table 1). Moreover, consistent with the domain distance, grazing-incidence small-angle X-ray scattering (GISAXS) reveals the primary characteristic peak at the wavenumber $q = 0.14$ nm^{-1}, associated with a length scale of 44.8 nm (arrow in Figure 2c and Figure S3c). These results confirm that the ABA bottlebrush-based triblock copolymers form a physically cross-linked network, in which the cross-links are spherical hard glassy domains formed by linear PBnMA, whereas the network strands are soft elastic bottlebrush PDMS.

We use a stress-controlled rheometer to quantify the dynamic mechanical properties of the polymer network. Reminiscent of a perfect rubber,[35] at room temperature, the network exhibits a nearly frequency-independent shear storage modulus G', as shown by red circles in Figure 2d. Therefore, we take the value of G' at the lowest oscillatory shear frequency, 0.1 rad/s, as the equilibrium shear modulus G. The modulus is about 6 kPa, more than 30 times lower than the entanglement modulus, 200 kPa, of linear PDMS.[35] Moreover, the measured stiffness is consistent with the theoretical prediction for an unentangled polymer network: $G \approx kTN_A\rho/M = 4000$ Pa, where k is the Boltzmann constant, $T = 293$ K is the absolute temperature, N_A is the Avogadro number, $\rho \approx 1$ g/cm^3 is the density of PDMS, and $M = 600$ kg/mol is the mass of the triblock copolymer. As established in a recent study,[32] in addition to the elongation at break measured by tensile tests, the extensibility of a polymer network can be described by shear fracture strain γ_s, a parameter measured by large amplitude oscillatory shear (LAOS).[36] Above γ_s, the network fractures such that the storage modulus becomes smaller than the loss modulus. The self-assembled network exhibits a fracture strain $\gamma_s = 1.66$, as shown in Figure 2e. These results indicate that the self-assembled network is a soft, stretchable elastomer.

Unlike conventional elastomers in which the cross-links are permanent chemical bonds, in the self-assembled network, the cross-links are glassy domains, which are physical bonds and

https://doi.org/10.1021/acs.chemmater.0c04659
Chem. Mater. 2021, 33, 2436−2445

expected to dissociate either at high temperature or in the presence of solvents. To explore this, we monitor in real time the viscoelasticity of the network from −20 °C to 180 °C. At an oscillatory shear frequency of 1 rad/s, the network remains a solid with G' nearly 10 times larger than G'' (Figure S4a). Consistent with this, up to 180 °C, the network exhibits no changes in microstructure, as shown by the characteristic scattering peaks at fixed wavenumbers from *in situ* GISAXS measurements in Figure 2c. However, slightly increasing the temperature to the melting point of PBnMA polymers, 200 °C, results in vanished characteristic scattering peaks (black line in Figure 2c), suggesting the dissociation of the glassy domains. This behavior is similar to classical thermoplastic elastomers,[37,38] which are solid at temperature below the melting point of the glassy domains, but compared with them, our elastomers are more than 1000 times softer.

Interestingly, the stiffness of the self-assembled network decreases with the increase in temperature, and such a behavior exhibits three regimes, as shown in Figure 2f. In regime I with the temperature below the glass transition temperature of PBnMA, $T < T_1 \sim T_{g,PBnMA} = 54$ °C, G' decreases very slowly by less than 5%. In regime II above $T_{g,PBnMA}$, $T_1 < T < T_2 \sim 120$ °C, G' decreases dramatically by more than 50% from nearly 8500 to 3500 Pa; in regime III with $T > T_2$, the decrease in G' slows down again with less than 5% up to 180 °C. A similar trend is confirmed by the dependence of equilibrium shear modulus on temperature (Figure S4b). This behavior contrasts with a chemically cross-linked polymer network whose equilibrium modulus proportionally increases with temperature.

The three distinct regimes are likely attributed to different molecular mechanisms. Similar to typical thermoplastic elastomers, the slow, small decrease is dominated by the accelerated relaxation of polymers upon heating such that it decreases the number of modes with relaxation time scales at or shorter than 2π seconds, the time scale at which the measurements are performed.[39] The fast, dramatic decrease, however, likely is dominated by changes in network topology. Above $T_{g,PBnMA}$, the PBnMA chains can pull out from the spherical domains;[40−42] this would result in not only a dramatic decrease in the amount of elastically effective network strands and thus network modulus but also an increase in energy loss associated with chain arrangement, as reflected by the increase in loss modulus (blue dashed line in Figure S4a). Importantly, up to 180 °C, the physical network remains to be a good elastomer with G' being much larger than G'' over a wide range of oscillatory shear frequency from 0.1 to 100 rad/s (hexagrams in Figure 2d). Such thermostability is appealing for applications in harsh environments but poses challenges in applying the material for direct-write 3D printing.

As an alternative, we explore the effects of solvents on the dynamic mechanical properties of the elastomer. Before and after solvent reprocessing, the elastomer exhibits a negligible difference in the viscoelasticity over a wide range of frequency, suggesting that the material is nearly 100% reprocessable (Figure S4c). By gradually decreasing the amount of solvent, we find that when dissolved in dichloromethane (DCM) at a 1:2 volume ratio, the mixture becomes a yield stress fluid: it is an elastic solid with a shear modulus of 300 Pa but becomes liquid-like above shear stress 70 Pa, as shown in Figure 2g. This is likely because the solvent swells the spherical domains such that the PBnMA chains can be pulled out under shear stress, resulting in the dissociation of the network. However, once the stress is released, the triblock copolymers re-assemble to form a solid network. Such a yield stress behavior enables the materials for direct-write printing: it allows the material to flow through a printer nozzle under stress, but once the stress is released, the solid-like behavior provides mechanical support for the printed features.

Exploiting the stress yield behavior, we demonstrate that the soft elastomers are amenable to direct-write printing 3D deformable structures. The elastomers can be used to print features with a resolution of ∼0.2 mm, as visualized by the sharp edges of a printed UVA logo in Figure 3a. Importantly, the solvent is highly volatile and evaporates quickly such that the printed structure instantly solidifies and is mechanically strong enough to support itself, as evidenced by Figure 3b and Movie S1. Moreover, a good fidelity can be achieved when printing a 3D honeycomb structure (Figure S5). This contrasts with most soft material printing, which often requires a sacrificial supporting matrix to provide mechanical support and/or post-processing to completely solidify the printed features.[9,15] Furthermore, we print a cubic gyroid, a kind of 3D structure not only inaccessible by conventional molding but also has been rarely achieved for direct-write printing ultrasoft elastomers. The printed cubic gyroid exhibits a slightly tapered shape (Figure 3c and Movie S2); this is likely because of solvent evaporation-induced volume shrinkage. Compared with the bulk sample (red line in Figure 3e and Movie S3), the gyroid is two times softer and non-dissipative (Figure 3d) and exhibits a delayed strain-stiffening (blue line in Figure 3f and Movie S4). The measured stress−strain behavior of the gyroid is qualitatively captured by finite element analysis (FEA) but quantitatively different at intermediate strains (black line in Figure 3f). This is likely because of defects introduced in 3D printing, which results in a structural collapse under intermediate compression, as shown by the snapshots in Figure 3g and Movies S4 and S5. A systematic understanding of how printing conditions such as shear rates and solvent evaporation affect printed structures is beyond the scope of this work and will be the subject of further study. Nevertheless, our results demonstrate that the elastomers are amenable to *in situ* direct-write printing complex, elastic, and deformable 3D structures without the aid of sacrificial supporting matrix or post-curing.

To further explore the limit of soft elastomers in mechanical properties, we tune the MW of the bottlebrush block while maintaining the weight fraction of the end blocks below 6%. This ensures that the triblock copolymers form a sphere microstructure.[31] By increasing the middle bottlebrush block to 1500 kg/mol, we create a solvent-free elastomer with a shear modulus of 60 Pa (Table 1, sample S_{1500} in Figure S6a). This stiffness, by far, represents the lowest record of solvent-free elastomers and is comparable to the softest biological organ brain[22] and the elastic vocal cord tissue.[43] However, decreasing the middle block MW to 100 kg/mol does not increase the network stiffness; instead, it results in $G'' > G'$ and $G'' \sim \omega$, characteristics of a viscoelastic polymer liquid (sample S_{100} in Figure S6a).[35] This is because the MW of the end linear blocks 3000 g/mol is too small to form hard glassy domains. Interestingly, the measured network stiffness exhibits a non-monotonic dependence on polymer MW (symbols in Figure S6b). This is likely attributed to the formation of loops with two end linear blocks from the same triblock copolymer linking to the same spherical nodule, resulting in elastically ineffective network strands and thus reduced network stiffness. The probability of two ends to meet to form loops increases when the bottlebrush becomes either more flexible or shorter, at which the deviation of the measured

https://doi.org/10.1021/acs.chemmater.0c04659
Chem. Mater. 2021, 33, 2436−2445

network stiffness from the prediction becomes larger, as shown by the dashed line in Figure S6b. Nevertheless, by controlling the MW, the shear moduli of soft elastomers can be tuned over two orders of magnitude from ∼60 to ∼6000 Pa.

The extensibility of ultrasoft elastomers, in the form of shear fracture strain γ_s, decreases with the increase in shear modulus G (filled symbols in Figure 4a and Figure S6c). This is consistent with the classical understanding that the extensibility of polymer networks is proportional to the network strand size, which becomes smaller at higher network stiffness. Indeed, recently, it has been discovered[32] that the shear fracture strain of chemically cross-linked bottlebrush polymer networks is equal to the ratio of the contour length L_{max} to the end-to-end distance R of the bottlebrush between two neighboring cross-links: $\gamma_s = L_{max}/R - 1$, as shown by the empty symbols and the red line in Figure 4a. Both L_{max} and R are related to the network modulus G, and the molecular theory predicts two regimes: (i) for stiff bottlebrush polymers, γ_s is inversely proportional to the network shear modulus G, $\gamma_s \sim G^{-1}$; (ii) for flexible bottlebrush polymers, $\gamma_s \sim G^{-1/2}$, which recovers the behavior of conventional networks.[32] However, neither of these two scaling relations captures the behavior of the self-assembled network, whose extensibility exhibits a much weaker dependence on stiffness, $\gamma_s \sim G^{-1/4}$ (green line in Figure 4a). Moreover, at the same network stiffness, the self-assembled network is less stretchable than the chemically cross-linked bottlebrush polymer networks. Such a difference is likely because in the chemically cross-linked bottlebrush polymer network, the bottlebrush polymer is not pre-strained. By contrast, in the self-assembled network, to balance the interfacial free energy from the incompatible microdomains, the bottlebrush polymer must be pre-strained,[31] which would result in a less extensibility. However, the molecular origin of the scaling exponent $-1/4$ remains to be quantitatively understood. Nevertheless, these results highlight the importance of preventing pre-stretching of the bottlebrush network strands to achieve large extensibility.

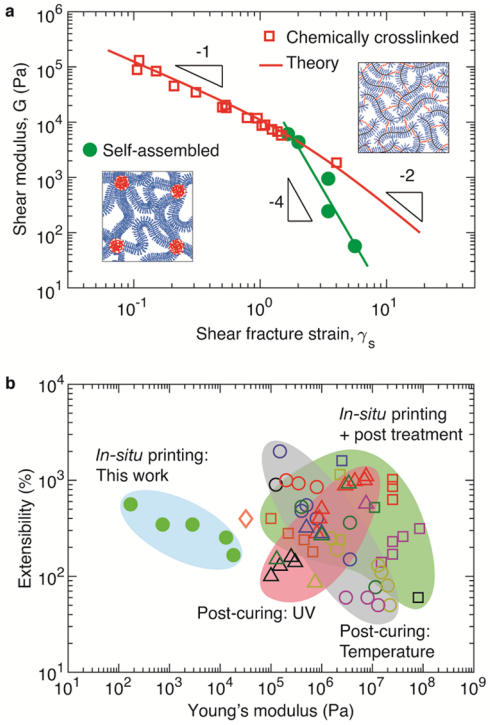

Figure 4. Mechanical properties of 3D printable elastomers. (a) Dependence of shear fracture strain, γ_s, on the shear modulus, G, of bottlebrush-based elastomers. Filled circles: elastomers formed by the self-assembly of PBnMA-bbPDMS-PBnMA triblock copolymers; empty circles: elastomers formed by chemically cross-linking in a melt precursor linear bottlebrush PDMS polymers of similar side chain grafting density and molecular weight (data from ref 32. Red line: theoretical prediction for the shear fracture strain of the chemically cross-linked bottlebrush polymer networks given by $\gamma_s = L_{max}/R - 1$, in which L_{max} and R are, respectively, the contour length and end-to-end distance of the bottlebrush polymer between two neighboring cross-links. Both L_{max} and R are determined by shear modulus G with exact relations detailed in ref 32. Green line: extensibility of the self-assembled elastomer scales with stiffness by a power of $-1/4$: $\gamma_s \sim G^{-1/4}$. (b) Ashby-type plot of 3D printable elastomers based on extensibility (shear fracture strain or elongation at break) and Young's modulus. The shear fracture strain measured by LAOS is equivalent to the elongation at break measured by elongation tests, as established in ref 32 and further demonstrated for samples S_{1000} and S_{1500} (Figure S7 and Movies S6 and S7). Filled symbols: ultrasoft elastomers; empty symbols: existing 3D printable elastomers (Table S1). The printed elastomeric structures require post-treatment: empty circles: post-curing by heat; empty triangles: post-curing by UV light; empty squares: thermoplastic elastomers that can be printed *in situ* but require post-treatment such as heat or light; empty diamond: a very recently reported 3D printable bottlebrush-based elastomer that requires post-curing by UV light.

CONCLUSIONS

Compared to all existing 3D printable elastomers (Table S1), our elastomers are more than two orders of magnitude softer (Figure 4b). Moreover, they can be stretched up to six times, as evidenced by both LAOS measurements (Figure S6c) and elongation tests (Figure S7 and Movies S6 and S7). The extreme softness originates from the bottlebrush molecular architecture, which prevents the formation of entanglements, whereas the stretchability is borne out of the large network strand size. Such molecular architecture-determined extreme mechanical properties are different from those of conventional polymer networks, which often involve using polymer liquids to swell the network to make it soft or using filler particles to increase the network extensibility; an example is modified silicone elastomers like Sylgard PDMS.[44] Moreover, our elastomers are different from very recently reported 3D printable photo-cross-linked bottlebrush-based elastomers. Technically, our elastomers are ∼100 times softer, dramatically pushing the limit in stiffness that solvent-free elastomers can reach. Conceptually, our elastomers are a kind of physically cross-linked network and stimuli-reversible, enabling instantaneous fixation of printed features without the need for post-treatment. This feature applies not only to the relatively stiff elastomer of ∼6000 Pa (Figure 3) but also to the very soft one of ∼200 Pa (Movie S8). Remarkably, our elastomers are of similar stiffness to 3D printable hydrogels[45−47] but contain no solvents (Figure S8 and Table S2); this may enable their applications in 3D bioprinting solvent-free, permanent scaffolds such as shape-morphing structures[48] and artificial vocal cords.[43] Thus, the extremely soft, stretchable, and reversible elastomers represent a new feedstock for direct-write 3D printing adaptive structures.

Although direct-write printing is of relatively low resolution compared with other techniques such as digital light processing-based 3D printing,[10,49,50] it enables transforming highly viscoelastic inks to multiple-material adaptive structures such as magnetic[18] and pneumatic[8] robots. Together with their solvent-reprocessability, our elastomers can be readily used as

https://doi.org/10.1021/acs.chemmater.0c04659
Chem. Mater. 2021, 33, 2436−2445

matrix materials to create functional polymer−nanoparticle composites for 3D printing.[51,52] Moreover, because the self-assembled elastomers are thermo-reversible, they can be used for temperature-assisted direct-writing printing,[16] which would avoid solvent evaporation-induced material defects for the printed structures. Finally, the design concept should be general and will enable the development of 3D printable reversible soft elastomers made of other polymers.

EXPERIMENTAL SECTION

Materials. MCR-M17 (monomethacryloxypropyl terminated polydimethylsiloxane, average molar mass of 5000 g/mol) was purchased from Gelest and purified using basic aluminum oxide columns to remove inhibitors before use. Benzyl methacrylate (96%), copper(II) chloride ($CuCl_2$, 99.999%), copper(II) bromide ($CuBr_2$, 99.999%), tris[2-(dimethylamino)ethyl]amine (Me_6TREN), ethylene bis(2-bromoisobutyrate) (2-BiB, 97%), tin(II) 2-ethylhexanoate ($Sn(EH)_2$, 92.5−100%), anisole (≥99.7%), and *p*-xylene (≥99.7%) were purchased from Sigma Aldrich and used as received. Toluene (Certified ACS), methanol (Certified ACS), diethyl ether (Certified ACS), dichloromethane (DCM, Certified ACS), dimethylformamide (DMF, Certified ACS), tetrahydrofuran (THF, Certified ACS), and THF (HPLC) were purchased from Fisher and used as received.

Polymer Synthesis and Characterization. To synthesize a linear-bottlebrush-linear triblock copolymer, we first synthesize the middle bottlebrush block and then use the bottlebrush as a macroinitiator to grow the end linear blocks. For both steps, we use activator regenerated by electron transfer (ARGET) atom transfer radical polymerization (ATRP),[53] as illustrated in Figure 1d. Here, we describe the detailed synthesis protocol using sample S_{500} as an example.

Step I: Synthesis of Bottlebrush Poly(dimethylsiloxane). A 50 mL Schlenk flask is charged with 2f-BiB (1.5 mg, 0.0042 mmol), MCR-M17 (10 g, 2 mmol), *p*-xylene (3.3 mL), and anisole (3.3 mL). We dissolve Me_6TREN (46 mg, 0.2 mmol) and $CuBr_2$ (4.5 mg, 0.02 mmol) in 1 mL of DMF to make a catalyst solution. Then, we add 30 μL of catalyst solution, containing 6×10^{-3} mmol Me_6TREN and 6×10^{-4} mmol $CuBr_2$, to the mixture and bubble it with nitrogen for 60 min to remove oxygen. Afterward, the reducing agent, $Sn(EH)_2$ (12.2 mg, 0.03 mmol) in 200 μL of *p*-xylene, is quickly added to the reaction mixture using a glass syringe. We seal the flask and then immerse it in an oil bath at 60 °C to start the reaction. The reaction is stopped after 3 h, and a small amount of mixture is taken out to determine the conversion by ^1H NMR (Figure S1). From ^1H NMR, the conversion is 18.5% and the degree of polymerization is 112 (see SI Text). This results in a bottlebrush polymer with a number average MW of 560 kg/mol.

The rest of the reaction mixture is diluted with THF and passed through a neutral aluminum oxide column to remove the catalyst. The collected solution is concentrated using a rotary evaporator (Buchi R-205). To separate the bottlebrush polymer from the unreacted macromonomers, we create a cosolvent, a mixture of methanol and diethyl ether with a volume ratio 3:2, which is a good solvent for the macromonomers but not for the bottlebrush PDMS. After precipitation, we further centrifuge the mixture to separate the polymer from the solvent and re-dissolve the separated polymer in THF to make a homogeneous solution. We repeat this precipitation procedure five times to ensure that all unreacted macromonomers and impurities are completely removed. We use GPC to measure the PDI of the final product, which is 1.41 for this bbPDMS (Figure S2a). At room temperature, bbPDMS is a viscous, colorless liquid.

Step II: Synthesis of LBBL Triblock Copolymers. A 50 mL Schlenk flask is charged with BnMA (906 mg, 5.14 mmol), macroinitiator (bbPDMS, 560 kg/mol, 1.34 g, 0.0024 mmol), *p*-xylene (3.9 mL), and anisole (2.6 mL). We dissolve Me_6TREN (46 mg, 0.2 mmol) and $CuCl_2$ (2.7 mg, 0.02 mmol) in 1 mL of DMF to make a catalyst solution. We add 64 μL of catalyst solution, containing 1.28×10^{-2} mmol of Me_6TREN and 1.28×10^{-3} mmol of $CuCl_2$, to the mixture and bubble it with nitrogen for 45 min to remove oxygen. Afterward, the reducing agent, $Sn(EH)_2$ (25.9 mg, 6.4×10^{-2} mmol) in 200 μL of *p*-xylene, is quickly added to the reaction mixture using a glass syringe. Then, we seal the flask and immerse it in an oil bath at 60 °C. The reaction is stopped after 2 h. The reaction mixture is diluted in THF and passed through a neutral aluminum oxide column to remove the catalyst, and the collected solution is concentrated using a rotavapor. Instead of using the cosolvent in step I, we use methanol for precipitation three times; this completely removes all unreacted monomers and impurities. After purification, the sample is dried in a vacuum oven (Thermo Fisher, Model 6258) at room temperature for 24 h. A small amount of the polymer is used for ^1H NMR analysis and GPC analysis. From ^1H NMR, the weight fraction is 6.4%, which indicates that the MW of PBnMA is about 19 kg/mol for each of the two end blocks. From GPC, the PDI is 1.52 for this triblock copolymer (Figure S2b). At room temperature, the polymer is a transparent, elastic solid.

Transmission Electron Microscopy. We use TEM to characterize the morphology of the self-assembled polymer networks. To ensure that the self-assembled microstructure is an equilibrium configuration, we use solvent-annealing to prepare the samples, during which the evaporation of the solvent is controlled at a slow rate. Specifically, an LBBL polymer is dissolved in toluene with a concentration of 5 mg/mL. The polymer solution is purified by passing through a syringe filter with a pore size 0.45 μm. Then, 10 μL of polymer solution is added to a carbon film-coated copper TEM grid, which is placed on a 1 mm-thick glass cover slide in a glass Petri dish partially filled with toluene. We cover the Petri dish with a glass lid to allow the solvent to slowly evaporate at room temperature for 36 h. The annealed sample is characterized using a hollow-cone dark-field TEM (FEI Titan) at an electron energy of 300 keV, and a representative image of sample S_{500} is shown in Figure 2b. We use ImageJ to calculate the PBnMA domain radius and the distance between the centers of neighboring PBnMA domains. The domain distance, *d*, and the domain radius, *r*, of sample S_{500} exhibit a normal distribution with $d = 49.2 \pm 4.7$ nm and $r = 10.2 \pm 1.2$ nm (Figure S4a,b).

Grazing-Incidence Small-Angle X-Ray Scattering. Using a synchrotron source at the 12-ID beamline in the Brookhaven National Laboratory, we perform GISAXS measurements to characterize the microstructure of the self-assembled polymers. The experiments are conducted in reflection geometry using an energy source of 13.9 keV. The distance between the sample and detector is 8.3 m.

To prepare thin films with controlled, uniform thicknesses, we use dynamic spin coating during which a polymer solution is dropped onto a silicon substrate rotating at a prescribed speed. For example, the sample S_{500} is dissolved in toluene with a concentration of 40 mg/mL. The polymer solution is purified by passing through a syringe filter with a membrane pore size 0.45 μm. In parallel, a 1 cm × 1 cm silicon wafer is loaded on a spin coater set with a rotation per minute (RPM) of 2000 and spin time of 40 s. After reaching a stable RPM, we drop 30 μL of polymer solution on the substrate. This results in a film of thickness 400 nm that is much larger than characteristic length scales of the self-assembled microstructure.

Rheometry. Rheological measurements are performed using a stress-controlled rheometer (Anton Paar MCR 302) equipped with a plate−plate geometry of a diameter 25 mm. We exploit the solvent reprocessability of LBBL polymers to prepare samples *in situ*. Specifically, we dissolve LBBL polymers in DCM at a volume ratio of 1:2 to make a homogeneous mixture. We pipette about 1 mL of solution onto the bottom plate, allow the solution to dry in the air at room temperature, and then heat the bottom plate to 40 °C for an additional 20 min. This allows us to prepare a relatively thick film, ∼0.3 mm, yet without the formation of cavities due to the evaporation of solvents. Then, we lower the upper plate and trim the excess sample at the edge of the geometry.

For frequency sweep, we fix the temperature at 20 °C and the oscillatory shear strain at 0.5% while varying the shear frequency from 0.1 to 100 rad/s. For strain sweep, we fix the temperature at 20 °C and the oscillatory shear frequency at 1 rad/s while increasing the shear strain from 1% to 1000%. For temperature sweep, we fix the oscillatory frequency at 1 rad/s and the shear strain at 5% while increasing the temperature from −20 °C to 180 °C, the highest temperature accessible by our rheometer. We use a slow temperature ramping rate, 1 °C /min,

https://doi.org/10.1021/acs.chemmater.0c04659
Chem. Mater. 2021, 33, 2436−2445

and wait for 20 min at each temperature point before collecting data; this ensures that the self-assembled microstructure is in equilibrium at each temperature point.

To characterize the yield stress behavior, we transfer the polymer mixture onto the bottom plate of the rheometer and then lower the upper plate to reach a 0.8 mm gap distance. Then, we add deionized water to the side of the mixture to prevent solvent evaporation. The density of DCM, 1.33 g/cm^3, is higher than that of water; this prevents convection-induced mixing. During the measurements, we fix the temperature at 20 °C and the oscillatory frequency at 1 Hz while increasing the shear stress from 1 to 160 Pa.

To demonstrate the reprocessability of the self-assembled elastomers, we dissolve the elastomer in DCM and re-dry the solution to obtain an elastomer. The solvent-reprocessed elastomer exhibits negligible changes in dynamic mechanical properties, as shown by Figure S4c.

Direct-Write Printing. To print the soft elastomers, we modify a fused deposition modeling printer (JGAURORA Z-603S, China) by replacing the printhead with a solution extrusion module. We load the stress yield polymer mixture in a 5 mL gastight glass syringe equipped with a dispensing needle of an inner diameter 0.25 mm. The G-code and printing speed is generated and optimized using slicing software Cura 14.07. We use sample S_{500} as the material for most printing tests because it is relatively easy to be synthesized in an amount large enough for 3D printing. However, all samples should be 3D printable because of their stimuli-reversibility, as indicated by printing a 3D ring using the second softest material S_{1000} (Movie S8).

Compression Tests. Because our elastomers are extremely soft, the force required to deform the material is very small. To this end, we use a rheometer (Anton Paar MCR 302) with a normal force resolution of 0.5 mN to perform the compression tests. The sample, in the form of either a bulk material or a printed cubic gyroid, is fixed onto the bottom geometry. We lower the upper geometry to contact with the sample, at which the normal force is slightly above 0. During the compression measurements, the moving profile of the upper plate is pre-setup to exert cyclic and subsequent large compression at a fixed strain rate 0.005/s. We record the normal force, gap size, and time and calculate the stress and strain based on the pre-measured dimensions of the samples.

Elongation Tests. The terminologies "extensibility" and "stretchability" are used interchangeably in literature to describe the extent to which a material can be deformed up to fracture. Typically, extensibility is measured as the elongation at break, or fracture strain, by tensile tests. Recently, using a combination of experimental and theoretical approaches, it has been demonstrated that, at low strain rates, the shear fracture strain measured by LAOS is equivalent to the elongation at break measured by tensile tests.[32]

To provide further evidence that the shear fracture strain is equivalent to the tensile strain, we perform elongation tests for the very soft samples, S_{1000} and S_{1500}. Because the amount of the samples is not enough for conventional tensile tests, we develop a customized elongation test by sandwiching a sample between two cylindrical rods facing each other, one of which is fixed in space, whereas the other is driven by a motorized linear translational stage, as illustrated in Figure S7a. We bring the two rods close to each other with a gap of ∼0.5 mm. In parallel, we dissolve the samples in DCM with a concentration about that used for 3D printing. We deposit into the gap about 20 μL of polymer solution; the wetting between the polymer solution and the surface of rods ensures that the solution fills the gap, whereas the rod−air−liquid interfacial tension balances gravitational force to prevent the liquid from falling off. After the solvent evaporates, we add the polymer solution again. We repeat this process to gradually build up the sample. This *in situ* sample preparation ensures a seamless contact between the rod and the sample, such that the adhesion between the two is strong enough to elongate the sample. During the elongation test, we control the strain rate at a low value of 0.01/s to avoid possible rate-dependent mechanical performance and use a camera to monitor the elongation in real time, as shown in Figure S7b,c and Movies S6 and S7. The elongation at break for S_{1500} is 5.96 and for sample S_{1000} is 3.15. These values are, respectively, consistent with the shear fracture strains, 5.62 and 3.46, measured by LAOS. Therefore, in this study, we use the shear fracture strain to describe the extensibility of polymer networks.

Finite Element Analysis (FEA). Using the ABAQUS/Standard package, we perform FEA simulation to model the response of 3D printed features under a quasi-static compression. The elastomer is described by the Neo Hooke model, in which the strain energy density is given by $W = C_{10}(I_1 - 3) + (1/D_1)(J - 1)^2$, where I_1 is the first strain invariant and J is the elastic volume ratio, which is defined by $J = \lambda_1\lambda_2\lambda_3$. λ_i (i = 1, 2, and 3) are the principal stretches. We calibrate the simulation by comparing it to the bulk sample (Figure 3e); this gives $C_{10} = 1.36 \times 10^{-2}$ and $D_1 = 0.32$. These parameters are used to simulate the gyroid, which is modeled by 24,000 four-node tetrahedral (C3D4) elements. For both the bulk and the gyroid, two rigid plates are added at two sides of a sample with a friction coefficient set to be 0.1.

■ ASSOCIATED CONTENT

Supporting Information

The Supporting Information is available free of charge at https://pubs.acs.org/doi/10.1021/acs.chemmater.0c04659.

Methods for ^{1}H NMR and GPC measurements; discussion on the effects of polymer molecular weight distribution; discussion on GISAXS results; ^{1}H NMR spectra of examples bbPDMS and LBBL polymers; GPC traces of all bbPDMS and LBBL polymers; microstructures of the self-assembled elastomers; dynamic mechanical properties of elastomers at various temperatures and after being reprocessed using solvents; optical image of a 3D printed honeycomb structure; effects of molecular weight on stiffness and extensibility; illustration and snapshots for customized elongation tests; comparison between ultrasoft elastomers and existing 3D printable hydrogels; and tables that summarize mechanical properties for existing 3D printable elastomers and hydrogels (PDF)

3D printing of UVA logo (MP4)

3D printing of cubic gyroid (MP4)

Compression test of the bulk sample (MP4)

Compression test of the 3D printed cubic gyroid (MP4)

Simulation of the compression test of cubic gyroid (MP4)

Elongation test of sample S_{1500} (MP4)

Elongation test of sample S_{1000} (MP4)

3D printing of a ring using sample S_{1000} (MP4)

■ AUTHOR INFORMATION

Corresponding Author

Li-Heng Cai − *Soft Biomatter Laboratory, Department of Materials Science and Engineering, Department of Chemical Engineering, and Department of Biomedical Engineering, University of Virginia, Charlottesville, Virginia 22904, United States;* orcid.org/0000-0002-6806-0566; Email: liheng.cai@virginia.edu

Authors

Shifeng Nian − *Soft Biomatter Laboratory, Department of Materials Science and Engineering, University of Virginia, Charlottesville, Virginia 22904, United States;* orcid.org/0000-0002-2243-6329

Jinchang Zhu − *Soft Biomatter Laboratory, Department of Materials Science and Engineering, University of Virginia, Charlottesville, Virginia 22904, United States*

Haozhe Zhang − *Department of Aerospace and Mechanical Engineering, University of Virginia, Charlottesville, Virginia 22904, United States*

https://doi.org/10.1021/acs.chemmater.0c04659
Chem. Mater. 2021, 33, 2436−2445

Zihao Gong − *Soft Biomatter Laboratory, Department of Materials Science and Engineering, University of Virginia, Charlottesville, Virginia 22904, United States*
Guillaume Freychet − *National Synchrotron Light Source-II, Brookhaven National Laboratory, Upton, New York 11973, United States*
Mikhail Zhernenkov − *National Synchrotron Light Source-II, Brookhaven National Laboratory, Upton, New York 11973, United States;* orcid.org/0000-0003-3604-0672
Baoxing Xu − *Department of Aerospace and Mechanical Engineering, University of Virginia, Charlottesville, Virginia 22904, United States;* orcid.org/0000-0002-2591-8737

Complete contact information is available at: https://pubs.acs.org/10.1021/acs.chemmater.0c04659

Author Contributions

#S.N. and J.Z. contributed equally.

Author Contributions

L.-H.C., S.N., and J.Z. designed the research. S.N., J.Z., H.Z., and Z.G. performed the research. S.N. synthesized and characterized the elastomers. J.Z., S.N., and Z.G. 3D printed the elastomers. H.Z. and B.X. performed finite element analysis for the compression of the 3D printed cubic gyroid. G.F. and M.Z. helped with GISAXS measurements and data analysis. L.-H.C. and S.N. wrote the paper. All authors reviewed and commented on the paper. L.-H.C. supervised the research.

Funding

L.-H.C. is supported by NSF CAREER DMR-1944625. This research used the SMI beamline (12-ID) of the National Synchrotron Light Source II, a U.S. Department of Energy (DOE) Office of Science User Facility operated for the DOE Office of Science by Brookhaven National Laboratory under contract no. DE-SC0012704.

Notes

The authors declare the following competing financial interest(s): L.H.C., S.N., J.Z., and Z.G. have filed a U.S. provisional patent application (No. 63/059,779; July 31, 2020) relating to 3D printable ultrasoft reversible elastomers.

■ ACKNOWLEDGMENTS

We thank Dr. Connie Roth, Dr. Jian Qin, and Dr. Ralph Colby for enlightening discussions.

■ REFERENCES

(1) Truby, R. L.; Lewis, J. A. Printing Soft Matter in Three Dimensions. *Nature* **2016**, *540*, 371−378.
(2) Gantenbein, S.; Masania, K.; Woigk, W.; Sesseg, J. P. W.; Tervoort, T. A.; Studart, A. R. Three-Dimensional Printing of Hierarchical Liquid-Crystal-Polymer Structures. *Nature* **2018**, *561*, 226−230.
(3) Oran, D.; Rodriques, S. G.; Gao, R.; Asano, S.; Skylar-Scott, M. A.; Chen, F.; Tillberg, P. W.; Marblestone, A. H.; Boyden, E. S. 3D Nanofabrication by Volumetric Deposition and Controlled Shrinkage of Patterned Scaffolds. *Science* **2018**, *362*, 1281−1285.
(4) Kelly, B. E.; Bhattacharya, I.; Heidari, H.; Shusteff, M.; Spadaccini, C. M.; Taylor, H. K. Volumetric Additive Manufacturing via Tomographic Reconstruction. *Science* **2019**, *363*, 1075−1079.
(5) Ligon, S. C.; Liska, R.; Stampfl, J.; Gurr, M.; Mülhaupt, R. Polymers for 3D Printing and Customized Additive Manufacturing. *Chem. Rev.* **2017**, *117*, 10212−10290.
(6) Tumbleston, J. R.; Shirvanyants, D.; Ermoshkin, N.; Janusziewicz, R.; Johnson, A. R.; Kelly, D.; Chen, K.; Pinschmidt, R.; Rolland, J. P.; Ermoshkin, A.; et al. Continuous Liquid Interface Production of 3D Objects. *Science* **2015**, *347*, 1349−1352.
(7) Walker, D. A.; Hedrick, J. L.; Mirkin, C. A. Rapid, Large-Volume, Thermally Controlled 3D Printing Using a Mobile Liquid Interface. *Science* **2019**, *366*, 360−364.
(8) Skylar-Scott, M. A.; Mueller, J.; Visser, C. W.; Lewis, J. A. Voxelated Soft Matter via Multimaterial Multinozzle 3D Printing. *Nature* **2019**, *575*, 330−335.
(9) Hinton, T. J.; Hudson, A.; Pusch, K.; Lee, A.; Feinberg, A. W. 3D Printing PDMS Elastomer in a Hydrophilic Support Bath via Freeform Reversible Embedding. *ACS Biomater. Sci. Eng.* **2016**, *2*, 1781−1786.
(10) Patel, D. K.; Sakhaei, A. H.; Layani, M.; Zhang, B.; Ge, Q.; Magdassi, S. Highly Stretchable and UV Curable Elastomers for Digital Light Processing Based 3D Printing. *Adv. Mater.* **2017**, *29*, 1606000.
(11) Scott, P. J.; Meenakshisundaram, V.; Hegde, M.; Kasprzak, C. R.; Winkler, C. R.; Feller, K. D.; Williams, C. B.; Long, T. E. 3D Printing Latex: A Route to Complex Geometries of High Molecular Weight Polymers. *ACS Appl. Mater. Interfaces* **2020**, *12*, 10918−10928.
(12) Wallin, T. J.; Simonsen, L. E.; Pan, W.; Wang, K.; Giannelis, E.; Shepherd, R. F.; Mengüç, Y. 3D Printable Tough Silicone Double Networks. *Nat. Commun.* **2020**, *11*, 4000.
(13) Kolesky, D. B.; Truby, R. L.; Gladman, A. S.; Busbee, T. A.; Homan, K. A.; Lewis, J. A. 3D Bioprinting of Vascularized, Heterogeneous Cell-Laden Tissue Constructs. *Adv. Mater.* **2014**, *26*, 3124−3130.
(14) Lee, A.; Hudson, A. R.; Shiwarski, D. J.; Tashman, J. W.; Hinton, T. J.; Yerneni, S.; Bliley, J. M.; Campbell, P. G.; Feinberg, A. W. 3D Bioprinting of Collagen to Rebuild Components of the Human Heart. *Science* **2019**, *365*, 482−487.
(15) Muth, J. T.; Vogt, D. M.; Truby, R. L.; Mengüç, Y.; Kolesky, D. B.; Wood, R. J.; Lewis, J. A. Embedded 3D Printing of Strain Sensors within Highly Stretchable Elastomers. *Adv. Mater.* **2014**, *26*, 6307−6312.
(16) Kotikian, A.; Truby, R. L.; Boley, J. W.; White, T. J.; Lewis, J. A. 3D Printing of Liquid Crystal Elastomeric Actuators with Spatially Programed Nematic Order. *Adv. Mater.* **2018**, *30*, 1706164.
(17) Schaffner, M.; Faber, J. A.; Pianegonda, L.; Rühs, P. A.; Coulter, F.; Studart, A. R. 3D Printing of Robotic Soft Actuators with Programmable Bioinspired Architectures. *Nat. Commun.* **2018**, *9*, 878.
(18) Kim, Y.; Yuk, H.; Zhao, R.; Chester, S. A.; Zhao, X. Printing Ferromagnetic Domains for Untethered Fast-Transforming Soft Materials. *Nature* **2018**, *558*, 274−279.
(19) Saed, M. O.; Ambulo, C. P.; Kim, H.; De, R.; Raval, V.; Searles, K.; Siddiqui, D. A.; Cue, J. M. O.; Stefan, M. C.; Shankar, M. R.; et al. Molecularly-Engineered, 4D-Printed Liquid Crystal Elastomer Actuators. *Adv. Funct. Mater.* **2019**, *29*, 1806412.
(20) Kuang, X.; Chen, K.; Dunn, C. K.; Wu, J.; Li, V. C. F.; Qi, H. J. 3D Printing of Highly Stretchable, Shape-Memory, and Self-Healing Elastomer toward Novel 4D Printing. *ACS Appl. Mater. Interfaces* **2018**, *10*, 7381−7388.
(21) Davidson, E. C.; Kotikian, A.; Li, S.; Aizenberg, J.; Lewis, J. A. 3D Printable and Reconfigurable Liquid Crystal Elastomers with Light-Induced Shape Memory via Dynamic Bond Exchange. *Adv. Mater.* **2020**, *32*, 1905682.
(22) Levental, I.; Georges, P. C.; Janmey, P. A. Soft Biological Materials and Their Impact on Cell Function. *Soft Matter* **2007**, *3*, 299−306.
(23) Murphy, S. V.; Atala, A. 3D Bioprinting of Tissues and Organs. *Nat. Biotechnol.* **2014**, *32*, 773−785.
(24) Yuk, H.; Lu, B.; Zhao, X. Hydrogel Bioelectronics. *Chem. Soc. Rev.* **2019**, *48*, 1642−1667.
(25) Zhang, Y. S.; Khademhosseini, A. Advances in Engineering Hydrogels. *Science* **2017**, *356*, eaaf3627.
(26) Cai, L.-H.; Kodger, T. E.; Guerra, R. E.; Pegoraro, A. F.; Rubinstein, M.; Weitz, D. A. Soft Poly(Dimethylsiloxane) Elastomers from Architecture-Driven Entanglement Free Design. *Adv. Mater.* **2015**, *27*, 5132−5140.
(27) Paturej, J.; Sheiko, S. S.; Panyukov, S.; Rubinstein, M. Molecular Structure of Bottlebrush Polymers in Melts. *Sci. Adv.* **2016**, *2*, e1601478.

(28) Daniel, W. F. M.; Burdyńska, J.; Vatankhah-Varnoosfaderani, M.; Matyjaszewski, K.; Paturej, J.; Rubinstein, M.; Dobrynin, A. V.; Sheiko, S. S. Solvent-Free, Supersoft and Superelastic Bottlebrush Melts and Networks. *Nat. Mater.* **2016**, *15*, 183−189.
(29) Reynolds, V. G.; Mukherjee, S.; Xie, R.; Levi, A. E.; Atassi, A.; Uchiyama, T.; Wang, H.; Chabinyc, M. L.; Bates, C. M. Super-Soft Solvent-Free Bottlebrush Elastomers for Touch Sensing. *Mater. Horiz.* **2020**, *7*, 181−187.
(30) Xie, R.; Mukherjee, S.; Levi, A. E.; Reynolds, V. G.; Wang, H.; Chabinyc, M. L.; Bates, C. M. Room Temperature 3D Printing of Super-Soft and Solvent-Free Elastomers. *Sci. Adv.* **2020**, *6*, eabc6900.
(31) Nian, S.; Lian, H.; Gong, Z.; Zhernenkov, M.; Qin, J.; Cai, L.-H. Molecular Architecture Directs Linear-Bottlebrush-Linear Triblock Copolymers to Self-Assemble to Soft Reprocessable Elastomers. *ACS Macro Lett.* **2019**, *8*, 1528−1534.
(32) Cai, L.-H. Molecular Understanding for Large Deformations of Soft Bottlebrush Polymer Networks. *Soft Matter* **2020**, *16*, 6259−6264.
(33) Krause, S.; Gormley, J. J.; Roman, N.; Shetter, J. A.; Watanabe, W. H. Glass Temperatures of Some Acrylic Polymers. *J. Polym. Sci., Part A: Gen. Pap.* **1965**, *3*, 3573−3586.
(34) Bates, F. S.; Fredrickson, G. H. Block Copolymer Thermodynamics: Theory and Experiment. *Annu. Rev. Phys. Chem.* **1990**, *41*, 525−557.
(35) Rubinstein, M.; Colby, R. H. *Polymer Physics*; Oxford University Press: Oxford, UK, 2003; pp. 282−294.
(36) Hyun, K.; Wilhelm, M.; Klein, C. O.; Cho, K. S.; Nam, J. G.; Ahn, K. H.; Lee, S. J.; Ewoldt, R. H.; McKinley, G. H. A Review of Nonlinear Oscillatory Shear Tests: Analysis and Application of Large Amplitude Oscillatory Shear (LAOS). *Prog. Polym. Sci.* **2011**, *36*, 1697−1753.
(37) Holden, G. Thermoplastic Elastomers. In *Rubber Technology*; Morton, M. Ed.; 1987; pp. 653−703. DOI: 10.1016/B978-0-323-35824-8.00024-4.
(38) Chen, Y.; Kushner, A. M.; Williams, G. A.; Guan, Z. Multiphase Design of Autonomic Self-Healing Thermoplastic Elastomers. *Nat. Chem.* **2012**, *4*, 467−472.
(39) Hiemenz, P. C.; Lodge, T. P. *Polymer Chemistry*; 2nd ed.; CRC Press: 2007; pp. 478−485, DOI: 10.1201/9781420018271.
(40) Seitz, M. E.; Burghardt, W. R.; Faber, K. T.; Shull, K. R. Self-Assembly and Stress Relaxation in Acrylic Triblock Copolymer Gels. *Macromolecules* **2007**, *40*, 1218−1226.
(41) Lu, J.; Bates, F. S.; Lodge, T. P. Remarkable Effect of Molecular Architecture on Chain Exchange in Triblock Copolymer Micelles. *Macromolecules* **2015**, *48*, 2667−2676.
(42) Peters, A. J.; Lodge, T. P. Comparison of Gel Relaxation Times and End-Block Pullout Times in ABA Triblock Copolymer Networks. *Macromolecules* **2016**, *49*, 7340−7349.
(43) Chan, R. W.; Titze, I. R. Viscoelastic Shear Properties of Human Vocal Fold Mucosa: Measurement Methodology and Empirical Results. *J. Acoust. Soc. Am.* **1999**, *106*, 2008−2021.
(44) Chen, Q.; Zhao, J.; Ren, J.; Rong, L.; Cao, P. F.; Advincula, R. C. 3D Printed Multifunctional, Hyperelastic Silicone Rubber Foam. *Adv. Funct. Mater.* **2019**, *29*, 1900469.
(45) Highley, C. B.; Rodell, C. B.; Burdick, J. A. Direct 3D Printing of Shear-Thinning Hydrogels into Self-Healing Hydrogels. *Adv. Mater.* **2015**, *27*, 5075−5079.
(46) Jungst, T.; Smolan, W.; Schacht, K.; Scheibel, T.; Groll, J. Strategies and Molecular Design Criteria for 3D Printable Hydrogels. *Chem. Rev.* **2016**, *116*, 1496−1539.
(47) Zhang, B.; Li, S.; Hingorani, H.; Serjouei, A.; Larush, L.; Pawar, A. A.; Goh, W. H.; Sakhaei, A. H.; Hashimoto, M.; Kowsari, K.; et al. Highly Stretchable Hydrogels for UV Curing Based High-Resolution Multimaterial 3D Printing. *J. Mater. Chem. B* **2018**, *6*, 3246−3253.
(48) Siéfert, E.; Reyssat, E.; Bico, J.; Roman, B. Bio-Inspired Pneumatic Shape-Morphing Elastomers. *Nat. Mater.* **2019**, *18*, 24−28.
(49) Traugutt, N. A.; Mistry, D.; Luo, C.; Yu, K.; Ge, Q.; Yakacki, C. M. Liquid-Crystal-Elastomer-Based Dissipative Structures by Digital Light Processing 3D Printing. *Adv. Mater.* **2020**, *32*, 2000797.
(50) Kuang, X.; Wu, J.; Chen, K.; Zhao, Z.; Ding, Z.; Hu, F.; Fang, D.; Qi, H. J. Grayscale Digital Light Processing 3D Printing for Highly Functionally Graded Materials. *Sci. Adv.* **2019**, *5*, eaav5790.
(51) Bockstaller, M. R.; Mickiewicz, R. A.; Thomas, E. L. Block Copolymer Nanocomposites: Perspectives for Tailored Functional Materials. *Adv. Mater.* **2005**, *17*, 1331−1349.
(52) Boley, J. W.; Van Rees, W. M.; Lissandrello, C.; Horenstein, M. N.; Truby, R. L.; Kotikian, A.; Lewis, J. A.; Mahadevan, L. Shape-Shifting Structured Lattices via Multimaterial 4D Printing. *Proc. Natl. Acad. Sci. U. S. A.* **2019**, *116*, 20856−20862.
(53) Matyjaszewski, K.; Jakubowski, W.; Min, K.; Tang, W.; Huang, J.; Braunecker, W. A.; Tsarevsky, N. V. Diminishing Catalyst Concentration in Atom Transfer Radical Polymerization with Reducing Agents. *Proc. Natl. Acad. Sci.* **2006**, *103*, 15309−15314.

https://doi.org/10.1021/acs.chemmater.0c04659
Chem. Mater. 2021, 33, 2436−2445